Available online at www.sciencedirect.com
ScienceDirect
Ceramics International 36 (2010) 1147–1153
CERAMICS INTERNATIONAL
www.elsevier.com/locate/ceramint

Short communication

Properties of sol–gel derived Al_2O_3–15 wt.% ZrO_2 (3 mol% Y_2O_3) nanopowders using two different precursors

A. Taavoni-Gilan [a], E. Taheri-Nassaj [a,*], R. Naghizadeh [b], H. Akhondi [a]

[a] Department of Materials Science and Engineering, Tarbiat Modares University, P.O. Box 14115-143 Tehran, Iran
[b] Department of Materials Science and Engineering, Iran University of Science and Technology, P.O. Box 16846-13114 Tehran, Iran

Received 12 May 2009; received in revised form 9 June 2009; accepted 7 October 2009
Available online 13 November 2009

Abstract

An alumina–15 wt.% zirconia (3 mol% yttria) nanopowder was synthesized by sol–gel method using salt and alkoxide as precursors. $Al(NO_3)_3{\cdot}9H_2O$, $ZrOCl_2{\cdot}8H_2O$ and $Y(NO_3)_3{\cdot}6H_2O$ were used as salt precursors and $Al(OC_4H_9)_3$ and $Zr(OC_4H_9)_4$ were used as alkoxide precursors. The dried gels of two precursors were heat treated in the range of 450–1350 °C. The powders produced by alkoxide precursors calcined at 750 °C were in the range of 15–75 nm, while those prepared by salt precursors had the size in the range of 30–90 nm. The former powders had a higher surface area and smaller mean pore diameter compared with the later powder, i.e. 152 m^2/g and 5.63 nm comparing with 121 m^2/g and 9.79 nm, respectively. Therefore phase transformation in the former occurred in lower temperatures.

Keywords: B. Electron microscopy; Composite materials; Sol–gel growth; Phase transitions

1. Introduction

Zirconia-toughened alumina (ZTA) is a desirable material for engineering applications, because of its high hardness, high wear resistance and high toughness [1]. It is well known that both the fracture toughness and the strength of alumina ceramics are improved significantly by the dispersion of 10–20 vol.% of metastable tetragonal (t) zirconia particles which transform into the stable monoclinic phase (m) under loading. To this purpose, the zirconia dispersed into the fine alumina powder may either be pure, un-stabilized ZrO_2 particles or better tetragonal partially stabilized ZrO_2 particles, usually using 3 mol% yttria to partially stabilize the tetragonal phase [2–9]. The extent of toughening achieved in these composites depends on the particle size of Al_2O_3 and ZrO_2, volume fraction of ZrO_2 retained in the metastable tetragonal phase as well as on the relative distribution of ZrO_2 in the matrix. While a finer particle size of both Al_2O_3 and ZrO_2 will not only enhance the chances of a uniform Al_2O_3 and ZrO_2 distribution, but it also increases the possibility of ZrO_2 being retained as metastable tetragonal phase. A major problem in achieving a high-density Al_2O_3–ZrO_2 composite is the coarsening of ZrO_2 particles during high temperature processing. The coarsening of ZrO_2 will not only adversely affect the densification behavior, but also will reduce the retained tetragonal ZrO_2 [8].

Consequently, one approach to make a homogeneous Al_2O_3–ZrO_2 composite is the use of synthesized Al_2O_3–ZrO_2 composite powders made by a sol–gel process that can be easily synthesized with homogeneous nano-sized powder. A significant factor to be considered is the type of precursors, i.e. salt or alkoxide, influencing the size of powder and therefore its size dependent properties as well as agglomeration and surface area. In this work, the Al_2O_3–15 wt.% ZrO_2 (3 mol% Y_2O_3) composite nanopowders were synthesized using salt and alkoxide precursors via sol–gel method.

2. Experimental procedure

2.1. Powder processing

2.1.1. Part A: salt precursors

Aqueous solutions of $Al(NO_3)_3{\cdot}9H_2O$ (Merck, 98.5%), $ZrOCl_2{\cdot}8H_2O$ (Merck, 99%) and $Y(NO_3)_3{\cdot}6H_2O$ (Sigma–Aldrich, 99.9%) were used as the starting materials. The mixed

* Corresponding author. Tel.: +98 21 82883306; fax: +98 21 82883381.
E-mail address: taheri@modares.ac.ir (E. Taheri-Nassaj).

0272-8842/$34.00
doi:10.1016/j.ceramint.2009.11.011

hydrogel was obtained by adding NH_4OH solution to the mixed aqueous solution maintained at 25 °C with continuous stirring. The viscosity of the batch gradually increased and finally set to an enblock gel. The gels were then aged at room temperature for 48 h. After aging, the gel was repeatedly washed with boiled distilled water to remove impurities and filtered. The filtered cake was dried at 40 °C for 48 h. The dried gel was calcined in the range of 450–1350 °C with a heating rate of 10 °C/min and then maintained for 4 h and milled in air media in a high-density polythene bottle for 48 h using high purity alumina balls. The Al_2O_3–ZrO_2 (Y_2O_3) was prepared with a composition of Al_2O_3–15 wt.% ZrO_2 (3 mol% Y_2O_3). The detailed process flow chart of powder preparation is shown in Fig. 1. For the rest of this paper, we use the label SA15Z alternatively for this type of powders prepared by salt precursor.

2.1.2. Part B: alkoxide precursors

To make the Al_2O_3–15 wt.% ZrO_2 (Y_2O_3) composite nanopowders with alkoxide precursors, 4.230 g of aluminum (III) sec-butoxide (Merck, 97%), 1.057 g of ethylene glycol monoethyl ether (Sigma–Aldrich, 99%) and 8.0 g of isopropanol (Merck, 99.5%) were mixed with constant stirring and refluxed at 90 °C for 4 h. After 0.5635 g of zirconium (IV) butoxide (Sigma–Aldrich, 80%) poured into the funnel, this was dripped into the stable alumina sol. and then 9.0 g of deionized water contained 0.014 g of $Y(NO_3)_3{\cdot}6H_2O$ was added to make the ZrO_2 (3 mol% Y_2O_3). The synthesized composite was left in a dry oven at 100 °C for 24 h. The dried gel was calcined in the range of 450–1350 °C with a heating rate of 10 °C/min and then maintained for 4 h and milled in air media in a high-density polythene bottle for 48 h using high purity alumina balls. The Al_2O_3–ZrO_2 (Y_2O_3) was prepared with a composition of Al_2O_3–15 wt.% ZrO_2 (3 mol% Y_2O_3). The detailed process flow chart of powder preparation is shown in Fig. 2. We use the label AA15Z interchangeably for the powders produced by alkoxide precursors.

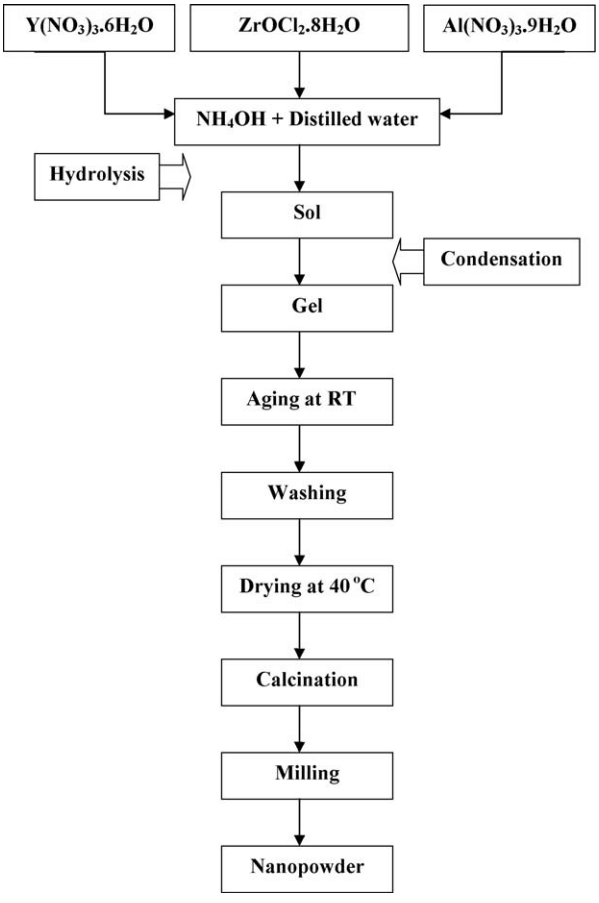

Fig. 1. The typical flow chart of the processing of Al_2O_3–ZrO_2 (Y_2O_3) nanopowder produced by salt precursors.

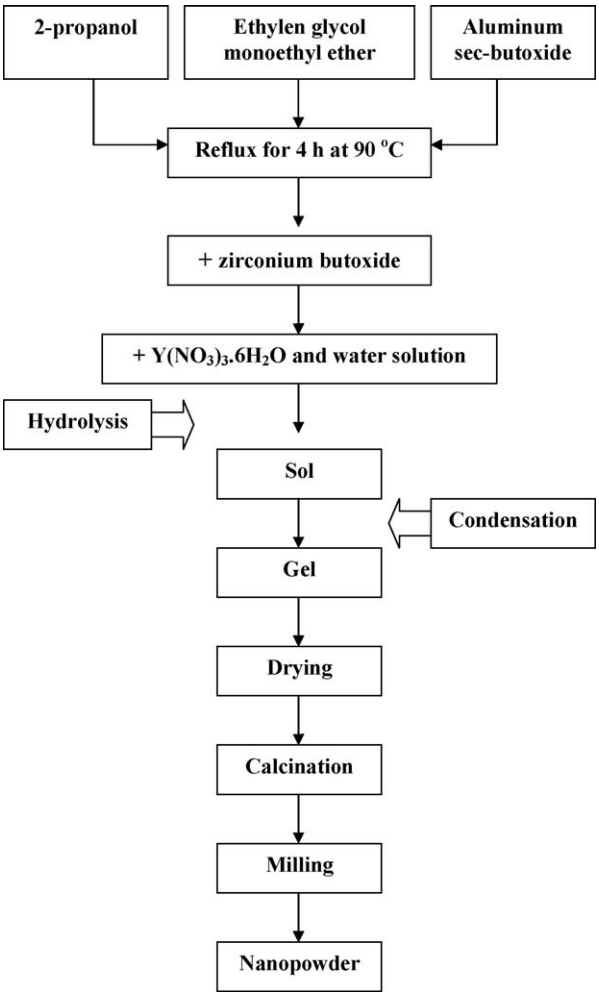

Fig. 2. The typical flow chart of the processing of Al_2O_3–ZrO_2 (Y_2O_3) nanopowder produced by alkoxide precursors.

2.2. Powder characterization

X-ray diffraction was carried out for phase analysis of the dried gel and calcined powder using Philips X'Pert model with Cu Kα radiation. Differential thermal analyses (DTA) and thermogravimetric (TG) were used in the range of 40–1200 °C with a heating rate of 10 °C/min with L60H1550 and STA 1460 equipments, respectively. The BET surface area and the pore size distribution of the calcined samples in air at 750 °C for 4 h were determined in a surface analyzer model (BEL Japan)

using N_2 as the adsorbate. FTIR analysis of dried gel and calcined powders was carried out in a Nicolet Nexus 6700 spectrometer in the wavenumber range 400–4000 cm^{-1} for studying the chemical groups on the surface of the as-dried gel as well as calcined powder. The powder morphology was investigated using a Philips XL30 scanning electron microscope.

3. Result and discussions

3.1. XRD analysis

The X-ray diffraction patterns of the gels heat treated for 4 h for salt and alkoxide precursors at temperature ranges from 450 to 1350 °C are shown in Figs. 3 and 4 and summarized in Table 1. Regarding these data, it is evident that the crystallization of the alkoxide sample, i.e. the formation of γ-Al_2O_3, is initiated at lower temperature than that of the salt precursor. X-ray diffraction could not clearly distinguish between gamma and delta alumina; therefore, gamma is used to denote both phases in the following text [10]. The same behavior is observed in the formation of subsequent phases of alumina and zirconia, i.e. the formation temperatures of t-ZrO_2 and α-Al_2O_3 phases are lower in alkoxide precursors comparing with the salt precursor. This phenomenon is due to higher specific surface

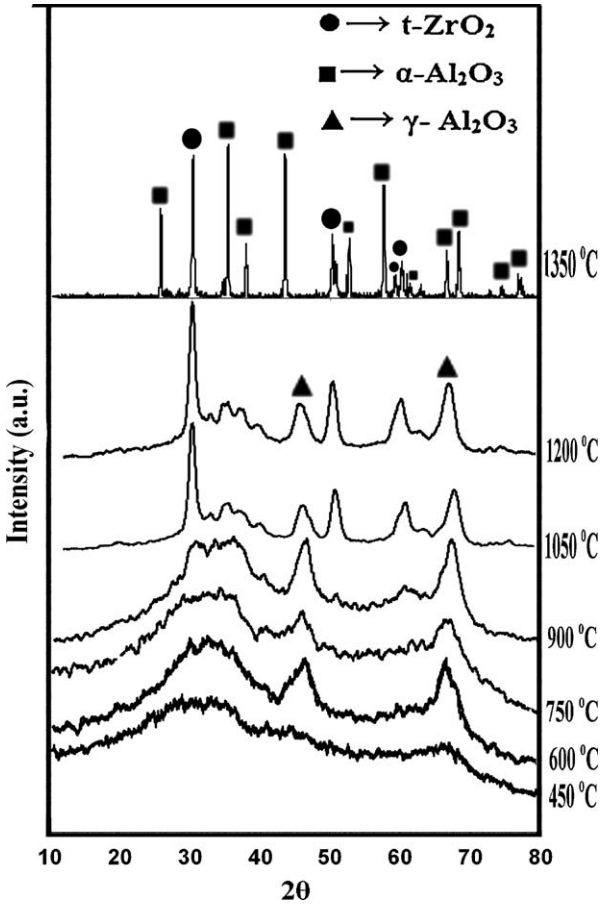

Fig. 3. Phase analysis of nanopowders produced by salt precursors calcined at different temperatures (SA15Z).

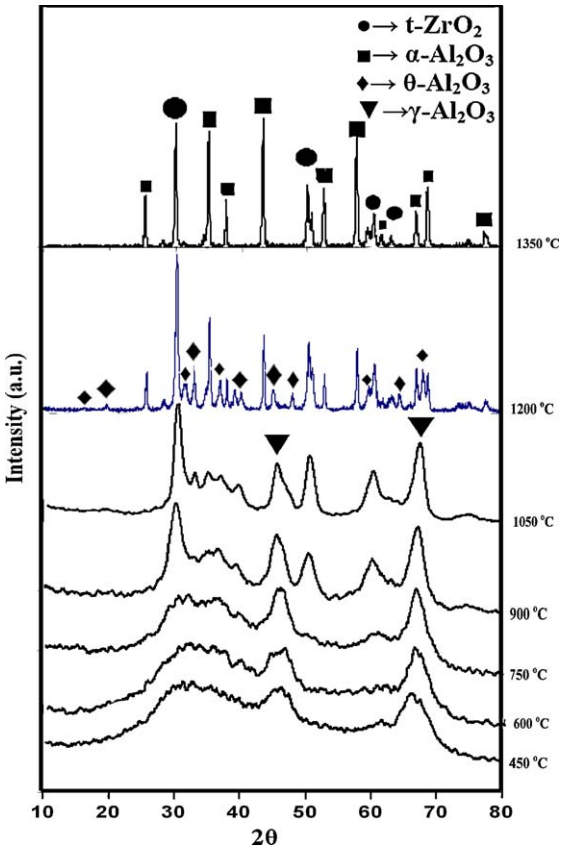

Fig. 4. Phase analysis of nanopowders produced by alkoxide precursors calcined at different temperatures (AA15Z).

area of nanopowder produced from alkoxide precursors compared to one produced from salt precursors [11–14]. The intensity of these phases increases up to 1350 °C. The formation of α-Al_2O_3 phase is completed at 1350 °C in both samples. As can be seen in Table 1, the transformation of transitional aluminas to α-alumina occurs at higher temperatures in the presence of zirconia. This has been explained by Doni Jayaseelan et al. [15].

3.2. Thermal behavior of hydrogel

The DTA and TG analyses of dried gels of salt and alkoxide precursors are shown in Figs. 5 and 6, respectively. In the SA15Z sample at the temperature range 40–240 °C DTA curve

Table 1
Phase identification of Al_2O_3–15 wt.% ZrO_2 (3 mol% Y_2O_3) nanopowders produced by salt and alkoxide precursors calcined at different temperatures.

Calcinations temperature (°C)	Phase identified by XRD	
	Alkoxide precursors	Salt precursors
450	γ-Al_2O_3	–
600	γ-Al_2O_3	γ-Al_2O_3
750	γ-Al_2O_3	γ-Al_2O_3
900	γ-Al_2O_3, t-ZrO_2	γ-Al_2O_3
1050	γ-Al_2O_3, t-ZrO_2	γ-Al_2O_3, t-ZrO_2
1200	θ, γ, α-Al_2O_3, t-ZrO_2	γ-Al_2O_3, t-ZrO_2
1350	α-Al_2O_3, t-ZrO_2	α-Al_2O_3, t-ZrO_2

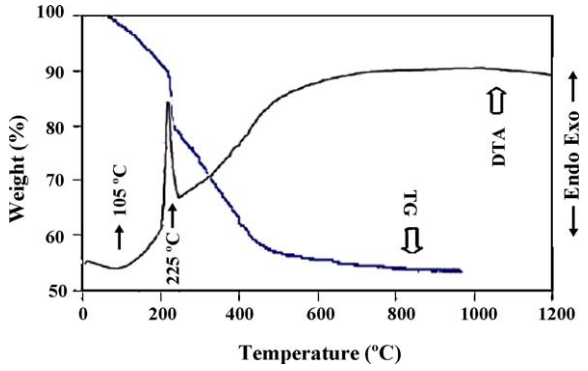

Fig. 5. TG/DTA plot for nanopowders produced by salt precursors in air (SA15Z).

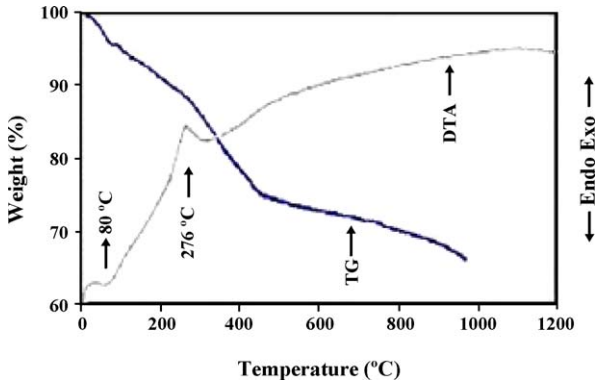

Fig. 6. TG/DTA plot for nanopowders produced with alkoxide precursors in air (AA15Z).

shows a broad endothermic peak at 105 °C and sharp exothermic peak at about 225 °C. The endothermic peak at 105 °C and the associated weight loss correspond to dehydroxylation of pseudoboehmite and expulsion of physically bonded water. The dehydroxylation of pseudoboehmite is associated with the crystallization of bayerite (β-$Al_2O_3{\cdot}3H_2O$). Thus, the exothermic peak at 225 °C and the associated weight loss could be related to the crystallization of bayerite [16]. Because of low content of this crystalline phase, XRD technique was unable to indicate it. The total weight loss appeared in the TG curve was 46%.

Fig. 6 shows the TG and DTA profiles of AA15Z sample. In the TG curve, the weight loss percentage measured was about 34% from room temperature to 970 °C. This result is attributed to the elimination of residual organic materials, e.g. ethylene glycol monoethyl ether, after the polymerization and the removal of by-products produced by the metal oxide formation process. In the DTA curve, a broad endothermic peak was detected at 80 °C, which was formed by incomplete

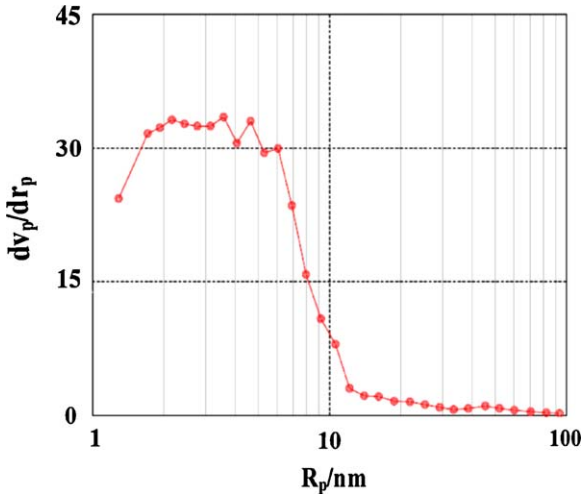

Fig. 7. Pore size distribution of the gel with salt precursors calcined at 750 °C for 4 h and milled for 48 h (SA15Z).

polymerization and residual organic materials. The exothermic peak at 276 °C corresponded to the formation of a metal oxide due to the elimination of organic materials in metal alkoxide.

The results of investigating and comparing TG and DTA curves of the two samples can be summarized as the following:

(i) Although in the two samples, the exothermic peaks related to crystallization were not observed in the temperature range from 300 to 1350 °C, XRD pattern of the gels showed the formation of crystalline phases (see Figs. 3 and 4).
(ii) The highest temperature for the SA15Z sample at which the increase of temperature happens together with weight loss is 800 °C, which is lower than the similar temperature for alkoxide sample.
(iii) The comparison of DTA curves of the samples shows that the beginning of the formation of metal oxide in AA15Z sample corresponds to lower temperatures comparing with the SA15Z sample, being consistent with XRD analyses of the samples. This phenomenon results from the smaller size of AA15Z powder and therefore its higher specific surface area in comparison with that of SA15Z powder.

3.3. Pore structure and pore size distribution

Specific surface BET areas of 152 and 121 m^2/g for alkoxide and salt precursors at 750 °C, were obtained (Table 2), respectively. The mean pore size distributions calculated by the BJH method for two precursors are shown in Figs. 7 and 8, respectively. The AA15Z powders had a higher surface area and

Table 2
Characteristics of Al_2O_3–15 wt.% ZrO_2 (3 mol% Y_2O_3) nanopowders produced by salt and alkoxide precursors calcined at 750 °C and milled for 48 h.

Sample type	Calcinations temperature (°C)	Specific surface area (m^2/g)	Pore area (m^2/g)	Mean pore diameter (nm)	Total pore volume (cm^3/g)
Alkoxide precursor	750 (4 h)	152	188.3	5.63	0.21
Salt precursor	750 (4 h)	121	134.02	9.79	0.29

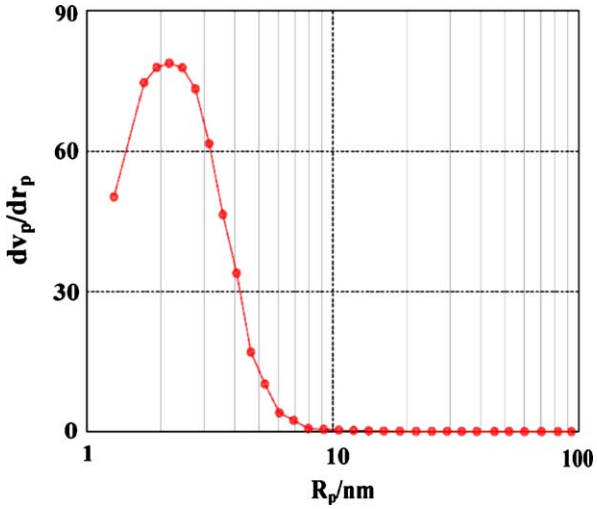

Fig. 8. Pore size distribution of the gel with alkoxide precursors calcined at 750 °C for 4 h and milled for 48 h (AA15Z).

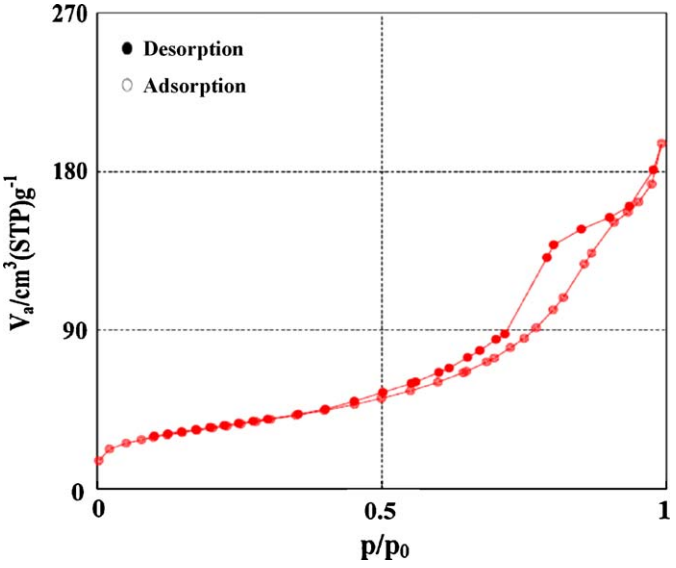

Fig. 9. Nitrogen adsorption/desorption of salt precursors calcined at 750 °C for 4 h and milled for 48 h (SA15Z).

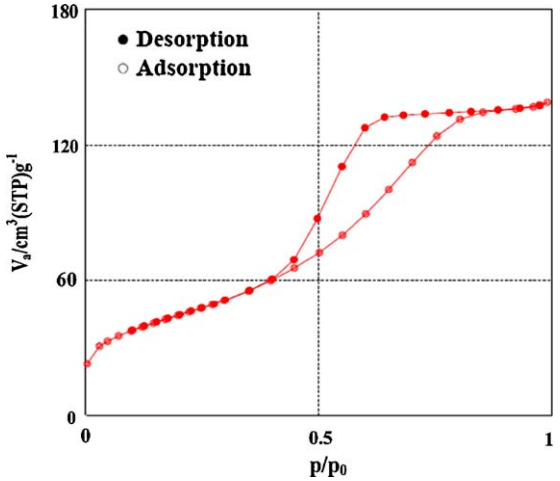

Fig. 10. Nitrogen adsorption/desorption of alkoxide precursors calcined at 750 °C for 4 h and milled for 48 h (AA15Z).

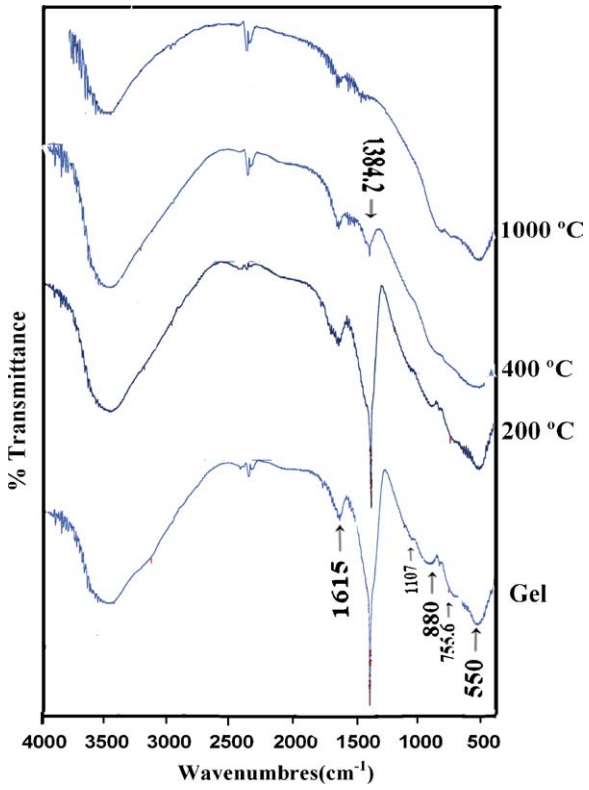

Fig. 11. FTIR curves of SA15Z sample: (a) dried gel, (b) 200 °C, (c) 400 °C and (d) 1000 °C.

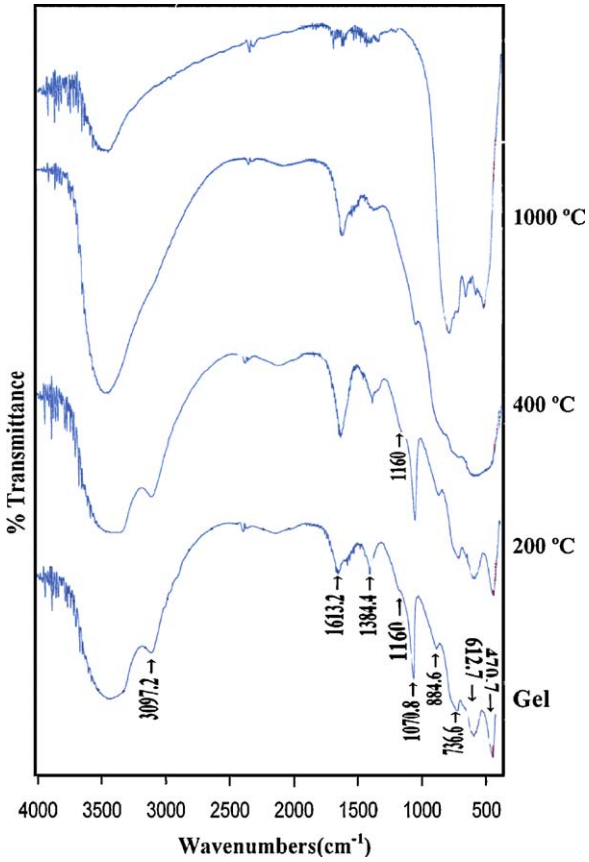

Fig. 12. FTIR curves of AA15Z sample: (a) dried gel, (b) 200 °C, (c) 400 °C and (d) 1000 °C.

smaller pore diameter compared to the SA15Z powders. The N_2 adsorption–desorption curves of the salt and alkoxide precursors at 750 °C show hysteresis loops and are shown in Figs. 9 and 10, respectively. The shape of the isotherm curves shows the characteristic behavior of the structure of powder, which is composed of an assembly of particles with large open packing. The hysteresis loops result from wedge-shaped capillaries with a closed edge at the narrower side [15,17,18]. The fact that, the difference between desorption and adsorption curves in the hysteresis loop in AA15Z is greater than that of in the SA15Z sample, may be ascribed to smaller pore size. Therefore, capillary effect in the AA15Z sample is more than that in the SA15Z sample [19,20].

3.4. FTIR analysis

The detailed IR spectra of the uncalcined hydrogels and calcined powders produced by salt and alkoxide precursors at different temperatures have been shown in Figs. 11 and 12, respectively. The gels and calcined samples exhibited –OH stretching vibration at wave numbers greater than 3000 cm^{-1}. The peak appeared in 3097 cm^{-1} at AA15Z sample is caused by C–H vibration of hydrocarbon groups [21]. The appeared peaks at 1615–1161 cm^{-1} for SA15Z and AA15Z samples are due to the bending vibration of Zr–OH groups. Another peak appears at 1161 cm^{-1}, which indicates the presence of more Zr–OH bonds in alkoxide batch. The appeared peaks at 1070 and 1107 cm^{-1} for alkoxide and salt precursors, are due to the presence of alumina gel [8], indicating the presence of hydrated groups. The above results conclude that alumina in this particular alumina–zirconia system is present as an intermediate bayerite [4]. Increasing the temperature leads to the reduction of intensities of the peaks and their disappearance at higher temperatures (1000 °C), resulting from the removal of hydroxide groups from the gels. The peaks between 1070 and 612 cm^{-1} in these two samples correspond to Al–O vibrations [22], being an additional peak in the alkoxide precursor than in the salt sample. This additional peak appeared at 612 cm^{-1}. The peak positions are more or less the same in two samples. The broadening absorption band at 520–500 cm^{-1} in SA15Z sample and the absorption band at 470 cm^{-1} in AA15Z sample correspond to Zr–O vibrations [6]. Heating at 400 °C causes broadening of peaks in the lower frequency range (500–1000 cm^{-1}) because of the overlapping of Al–O and Zr–O infrared vibrations of transition alumina and zirconia phases [8]. Thus, individual peaks corresponding to Zr–O could not be detected in the temperature range 200–400 °C. However, peaks corresponding to Al–O and Zr–O could be clearly observed at higher temperatures (1000 °C).

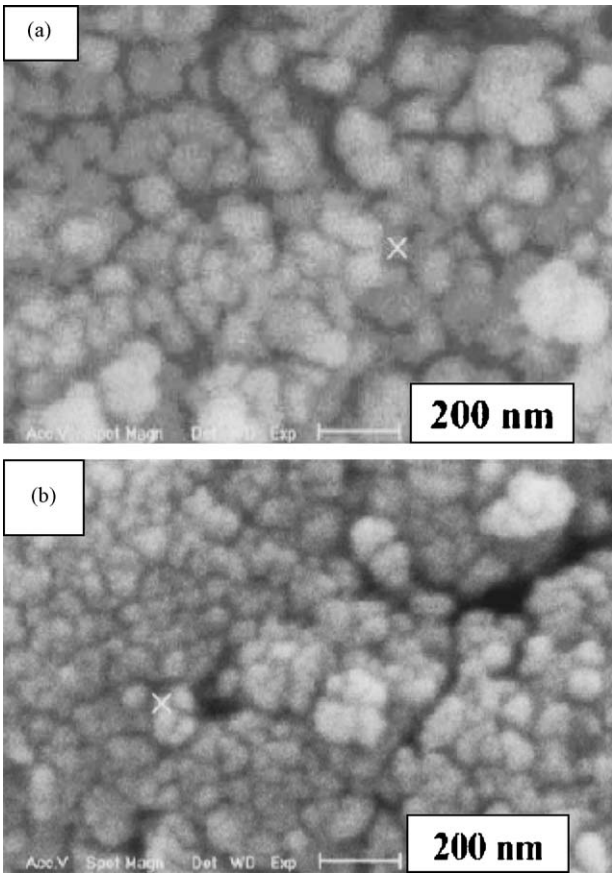

Fig. 13. SEM photographs of nanopowders calcined at 750 °C and milled for 48 h: (a) salt precursors (SA15Z) and (b) alkoxide precursors (AA15Z).

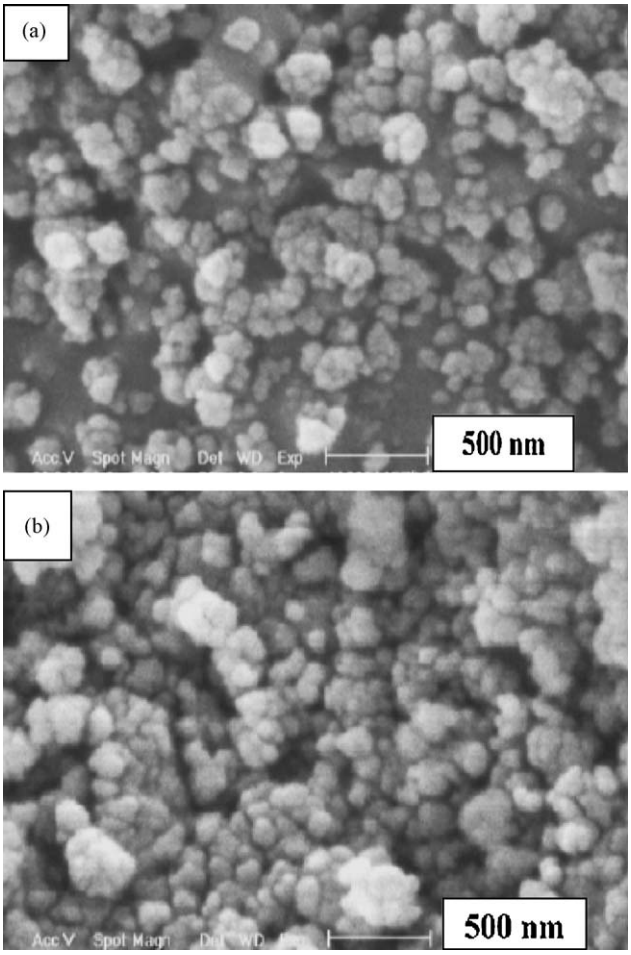

Fig. 14. SEM photographs of nanopowders calcined at 1200 °C and milled for 48 h: (a) salt precursors (SA15Z) and (b) alkoxide precursors (AA15Z).

The IR spectra relating to SA15Z and AA15Z samples show that a trace amount of –OH group still remains in the structure of ZrO_2 dispersed Al_2O_3 powder even after heating at 1000 °C, mainly due to the moisture absorption during testing [4].

3.5. SEM analysis

Fig. 13a and b shows the SEM micrographs of the SA15Z and AA15Z powders calcined at 750 °C. As shown, most of the particles have spherical shape and are in the range of 30–90 and 15–75 nm for SA15Z and AA15Z nanopowders, respectively. It is clearly observed that agglomeration of AA15Z nanopowders is higher than that of salt precursors. Fig. 14a and b shows that the particles of two samples began to sinter and agglomerate together with increasing calcination temperature to 1200 °C and agglomeration in AA15Z sample (Fig. 14b) is higher than that in SA15Z sample (Fig. 14a).

4. Conclusions

Al_2O_3–15 wt.% ZrO_2 (3 mol% Y_2O_3) nanopowders were synthesized by alkoxide and salt precursors. The results can be summarized as follows:

1. The SEM images show that the particle sizes of both samples are in the range of nanometer. The nanopowder produced by alkoxide precursors has smaller particle size than that produced by salt precursors.
2. The comparison of DTA curves of the two samples indicates that the beginning of the formation of alumina and zirconia phases in AA15Z sample corresponds to lower temperatures compared to the SA15Z sample.
3. The XRD analyses show that phase transformations of alumina and zirconia in alkoxide sample take place in lower temperatures comparing with the salt sample.
4. The BET analyses show that the alkoxide powders have higher surface area and smaller mean pore diameter compared to the salt powders.

References

[1] J.C. Debsikdar, Influence of synthesis chemistry on alumina–zirconia powder characteristics, Journal of Materials Science 22 (1987) 2237–2247.

[2] B.T. Lee, J.K. Han, F. Saito, Microstructure of sol–gel synthesized Al_2O_3–ZrO_2 (Y_2O_3) nano-composites studied by transmission electron microscopy, Journal of Materials Letters 59 (2005) 355–360.

[3] J.S. Hong, S.D. De la Torre, K. Miyamoto, H. Miyamoto, L. Gao, Crystallization of Al_2O_3/ZrO_2 solid solution powders prepared by coprecipitation, Materials Letters 37 (1998) 6–9.

[4] D. Sarkar, D. Mohapatra, S. Ray, S. Bhattacharyya, S. Adak, N. Mitra, Synthesis and characterization of sol–gel derived ZrO_2 doped Al_2O_3 nanopowder, Ceramics International 33 (2007) 1275–1282.

[5] Y.M. Kong, H.E. Kim, H.W. Kim, Production of aluminum–zirconium oxide hybridized nanopowder and its nanocomposite, Journal of the American Ceramic Society 90 (2007) 298–302.

[6] T. Noma, A. Sawaoka, Fracture toughness of high pressure sintered Al_2O_3–ZrO_2 ceramics, Journal of Materials Science Letters 3 (1984) 533–536.

[7] K. Matsui, M. Ohgai, Formation mechanism of hydrous zirconia particles produced by the hydrolysis of $ZrOCl_2$ solutions. III. Kinetics study for the nucleation and crystal-growth processes of primary particles, Journal of the American Ceramic Society 84 (2001) 2303–2312.

[8] R.P. Rana, S.K. Pratihar, S. Bhattacharyya, Powder processing and densification behavior of alumina-high zirconia nanocomposites using chloride precursors, Journal of Materials Processing Technology 190 (2007) 350–357.

[9] M.L. Balmer, F.F. Lange, C.G. Levi, Metastable phase selection and partitioning for $Zr(1-x)Al(x)O(2-x/2)$ materials synthesized with liquid precursors, Journal of the American Ceramic Society 77 (1994) 20693–20775.

[10] J. Kuo, D.L. Bourell, Structural evolution during calcination of sol–gel synthesized alumina and alumina–8 vol% zirconia composite, Journal of Materials Science 32 (1997) 2687–2692.

[11] R.C. Garvie, The occurrence of metastable tetragonal zirconia as a crystallite size effect, Physics & Chemistry 69 (1965) 1238–1243.

[12] F.F. Lange, Transformation toughening, Journal of Materials Science 17 (1982) 225–234.

[13] G. Gongyi, C. Yuli, Effect of preparation methods and condition of precursors on the phase composition of yttria-stabilized zirconia powders, Journal of the American Ceramic Society 75 (1992) 1294–1296.

[14] Y. Murase, E. Kato, K. Daimon, Stability of ZrO_2 phases in ultrafine ZrO_2–Al_2O_3 mixtures, Journal of the American Ceramic Society 69 (1986) 83–87.

[15] D. Doni Jayaseelan, D. Amutha Rani, T. Nishikawa, H. Awaji, Powder characteristics, sintering behavior and microstructure of sol–gel derived ZTA composites, Journal of the European Ceramic Society 20 (2000) 267–275.

[16] D Sarkar, S. Adak, N.K. Mitra, Preparation and characterization of an Al_2O_3–ZrO_2 nanocomposite. Part I. Powder synthesis and transformation behavior during fracture, Composites 38 (2006) 124–131.

[17] S. Brunauer, P.H. Emmett, E. Teller, Adsorption of gases in multimolecular layers, Journal of the American Chemistry Society 60 (1938) 309–319.

[18] A. Taavoni-Gilan, E. Taheri-Nassaj, H. Akhondi, The effect of zirconia content on properties of Al_2O_3–ZrO_2 (Y_2O_3) composite nanopowders synthesized by aqueous sol–gel method, Journal of Non-Crystalline Solids 355 (2009) 311–316.

[19] J.W. McBain, An explanation of hystersis in the hydration and dehydration of gels, Journal of the American Ceramic Society 57 (1935) 699–700.

[20] E.P. Barrett, L.G. Joyner, P. Halenda, The determination of pore volume and area distributions in porous substance. I. Computations from nitrogen isotherms, Journal of the American Chemistry Society 73 (1951) 373–380.

[21] K.R. Pachler, F. Matlok, K.U. Gremlich, Merck FT-IR Atlas; A Collection of FT-IR Spectra, VCH, 1988,, p. 520.

[22] Ph. Colomban, Structural of oxide gels and glasses by infrared and raman scattering, Journal of Materials Science 24 (1989) 3002–3010.